PCCP

Accepted Manuscript

This is an *Accepted Manuscript*, which has been through the Royal Society of Chemistry peer review process and has been accepted for publication.

Accepted Manuscripts are published online shortly after acceptance, before technical editing, formatting and proof reading. Using this free service, authors can make their results available to the community, in citable form, before we publish the edited article. We will replace this *Accepted Manuscript* with the edited and formatted *Advance Article* as soon as it is available.

You can find more information about *Accepted Manuscripts* in the **Information for Authors**.

Please note that technical editing may introduce minor changes to the text and/or graphics, which may alter content. The journal's standard **Terms & Conditions** and the **Ethical guidelines** still apply. In no event shall the Royal Society of Chemistry be held responsible for any errors or omissions in this *Accepted Manuscript* or any consequences arising from the use of any information it contains.

www.rsc.org/pccp

ARTICLE TYPE

Understanding the Interfacial Behavior in Isopycnic Lennard-Jones Mixtures by Computer Simulations[†]

José Matías Garrido[*a], Manuel M. Piñeiro[b], Andrés Mejía[a], and Felipe J. Blas[c]

The physical characterization of the singular interfacial behavior of heterogeneous fluid systems is a very important step in preliminary process design stages, and also in the subsequent procedures as the determination of the optimal operating conditions. Molar isopycnicity or molar density inversion is a special case of phase equilibrium behavior that directly affects the relative position of phases in heterogeneous mixtures, without being affected by gravitational fields. This work is dedicated to characterize the impact of molar density inversions on the interfacial properties of Lennard-Jones binary mixtures. Results and specific trends of the molar density inversion phenomena on the peculiar calculated composition profiles across the interface and interfacial tensions are explored by using canonical Molecular Dynamics Simulations of the Lennard-Jones binary mixtures. Our results show that the density inversion causes a drastic change in the density profile of the mixture. Specifically, symmetrical and equal-sized Lennard-Jones mixtures always exhibit desorption along the interfacial zone, *i.e.* the interfacial concentration profiles show *a relative minimum at the interface* of the total density profile, that increases when the dispersive energy parameter (ε_{ij}) between unlike species decrease. However, as the asymmetry of the Lennard-Jones mixtures increases ($\sigma_i \neq \sigma_j$), the concentration profiles display *a relative maximum at the interface*, which implies the adsorption of the total density profile along the interfacial zone.

1 Introduction

Phase density inversion phenomena are special cases of phase equilibrium behavior which occur in response to changes in variables that control the phase equilibrium (*i.e.* temperature and pressure), producing a change in the concentration of the phases, and subsequently also in phase density. As early as 1906, the physical phenomenon of density inversion was discovered by Kamerlingh Onnes[1] at the Leiden Physics Laboratory, when liquefying the helium + hydrogen mixture at 20 K and after 50 atm, Kamerlingh Onnes noted that upon increasing pressure, the gas phase mainly composed of helium became heavier than the hydrogen-rich liquid phase, leaving the first trapped in the bottom of the working cell. On one hand, the change of the relative position of phases observed in heterogeneous mixtures exposed to gravitational fields, is denoted as *Barotropy* or *mass density inversion*[1–6], and on the other hand, *Isopycnicity* in the case of *molar density inversion*[7–9] occurs when two phases of a heterogeneous mixture invert, independently of gravitational fields.

A heterogeneous mixture is said to be in molar isopycnic equilibrium when -at least- two of the constituent phases (*i.e.* α- and β-phases) are characterized by the same molar volume ($v^{\alpha} = v^{\beta}$) or, equivalently, by the same molar density ($\rho^{\alpha} = \rho^{\beta}$).[8,9] As follows from the previous definition, and considering that the density of the phases that compose a heterogeneous system become equivalent as critical states are approached, every critical point may be also defined as isopycnic.[9] However, in addition to these trivial cases -that can be clearly described along critical phase transitions- sub-critical isopycnic phase transitions are a case of anomalous equilibrium observed in heterogeneous mixtures, even including potentially attractive fluids that are gaining continuous interest in modern technological applications.

The behavior of heterogeneous mixtures at isopycnic phase equilibrium has been described by Quiñones-Cisneros[8] for a subset of Type III systems which, on the one hand, are composed by extremely asymmetric constituents and, on the other hand, tend to exhibit high temperature fluid-fluid equilibrium (*a.k.a.* gas-gas equilibrium[3,10]). The presence of isopycnic phase equilibrium has been confirmed for similar Type III mixtures by applying different Equation of State (EoS) models[11–15] to a set of key industrial mixtures, namely: refrigerant-lubricant mixtures,[16] mixtures composed by extremely asymmetric normal alkanes[17,18] or natural gastype mixtures, carbon dioxide + n-alkane mixtures[19,20] -

[a] *Dpto. de Ingeniería Química, Univ. de Concepción, POB 160-C, Concepción, Chile.*
[b] *Dpto. de Física Aplicada, Fac. de Ciencias, Univ. de Vigo, E36310, Spain.*
[c] *Laboratorio de Simulación Molecular y Química Computacional, CIQSO-Centro de Investigación en Química Sostenible y Departamento de Física Aplicada, Universidad de Huelva, E21071 Huelva, Spain.*
[*] *Corresponding author, e-mail: josemagarrido@udec.cl*

which comprise the backbone of oil reservoir engineering operations-, mixtures of carbon dioxide + commercial lubricants -which provide the technological basis of trans-critical refrigeration cycles [19] -, mixtures composed by water + hydrocarbons of large molecular weight [21–23] and for the case of perfluoroalkane + alkane mixtures. [24]
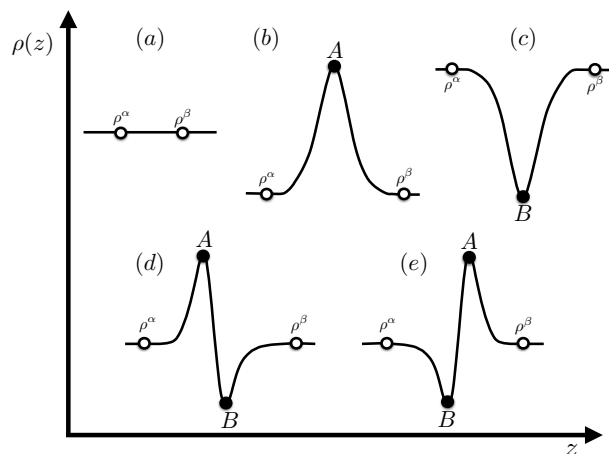

Fig. 1 Schematic $\rho - z$ projection of singular structures characterized at molar isopycnicity condition. (Open circles) represent the bulk phases (ρ^α and ρ^β) at isopycnicity condition; (filled circles) correspond a maximum (point A) and minimum (point B) observed along the density profiles.

Interestingly, for each of the previously mentioned examples, isopycnic phase behavior is either observed in the vicinity of a critical end point (CEP) of liquid-liquid-gas immiscibility or close to a vapor-liquid critical point. In addition, barotropy [4,6] can also be observed in the quoted isopycnic mixtures, suggesting a close link between the phenomena that directly influence the density of fluid mixtures and also the density gradient profiles in the case of liquid-liquid interfaces. In this context, the characterization and analysis of the evolution of the concentration profiles across the interfaces of binary systems that exhibit density inversion is very important due to the possible formation of special and unique interfacial structures directly related, that may represent a barrier to the mass transport between both bulk phases. [25–27] In spite of the impact that density gradients have on phase equilibrium, interfacial behavior and transport properties of heterogeneous mixtures have received limited attention so far, in thermo-physical conditions (*i.e.* temperature, pressure, composition) where density inversion phenomena becomes relevant in various technological applications. The analysis of isopycnicity has been limited mainly to its detection in predicted fluid-fluid equilibrium. Few previous works [9,28–30] have dealt with the characterization of the relation between isopycnic phase transitions, the Type of van Konynenburg and Scott [31] phase behavior, and

the drastic distortion of the mixtures density profiles in this kind of systems. Indeed, less attention has been devoted to the adsorption of fluid mixtures, where the phenomenon of preferential adsorption forms the basis of such practical applications as adsorptive separation of hydrocarbons. Experimental studies indicate that under appropriate thermodynamic conditions one can achieve a high degree of selectivity in the adsorption of a given component from the fluid mixture (for further details, the reader is referred for instance to Refs. 32–34). Following the thermodynamic conditions involved in phase density inversion (*a.k.a.* $\rho^\alpha = \rho^\beta$) we can distinguish in Fig. 1 five possibilities of how density inversion phenomena may affect the interfacial structure, modifying the behavior patterns of interfacial density profiles, without preferential adsorption and/or desorption. In this context, it is also important to mention that the interfacial behavior in Fig. 1 is based on the profile of the mixture and not in the partial density profiles of the components. On one hand, Fig. 1(a) shows the simplest case of a binary mixture without interfacial activity, where a completely flat profile between the bulk ρ^α- and ρ^β-phases is observed, case in which is likely that density gradients have no impact on transport properties. [35] On the other hand, as shown in Figs. 1(b) and 1(c) the maximum (point A) and minimum (point B) observed along the interfacial length clearly demonstrate that the total profile in the mixture is distorted with respect at the bulk phases (α and β). Finally, the other two possibles cases show either adsorption or desorption processes within the interface, represented by points of maximum and minimum activity (Fig. 1(d)) or systems with minimum and maximum activity (Fig. 1(e)) simultaneously, and they may represent an obstacle to mass transport through the phase boundary. In fact, the mass flow is lower when interfacial strength increases. [36] Therefore, the importance of analyzing the interfacial structure is emphasized by the related ability to identify sites and barriers to solute transport across the interface [37,38]. The resistance at the interface is determined by two effects [39,40]: (1) the decrease in hydrodynamic mobility and therefore diffusion in the vicinity of a fluid-fluid interface and (2) the existence of molecular interactions that produce the special interfacial properties, given by the distance of interaction between molecules.

The general objective of this contribution is discussing a two-way approach methodology for effectively guiding molecular simulations of an ideal potential force field -*as in the case of Lennard-Jones fluids*-, which is based on an accurate EoS model [11] of the potential and its wide ability to predict reliable interfacial behavior of heterogeneous mixtures at isopycnic phase equilibrium. We test the physical significance and coherency of the density profiles obtained from molecular simulation calculations in terms of state variables (*i.e.* temperature, pressure, composition) and conformational parameters (*i.e.* mixing rules, intermolecular interactions, etc.).

The work is organized as follows. First, the principal details of Global Phase Diagrams for binary mixtures at isopycnic condition are described. Then, a brief recall of the simulation details follows. Results and Discussion are presented in the next section, and finally conclusions are summarized.

2 Theory and Molecular Methods

2.1 Isopycnicity in Binary Mixtures

A Global Phase Diagram (GPD) is a parametric plot that maps regions where EoSs predict mixtures characterized by similar equilibrium behavior.[31] Thus, constraining our attention to the specific features observed in phase diagrams over a wide range of temperature and pressure (namely: presence or absence of azeotropy and/or liquid phase miscibility, overall geometric characteristics of critical lines, etc), the equilibrium behavior of mixtures may be classified in terms the Types[41] found in the different regions of the GPD.
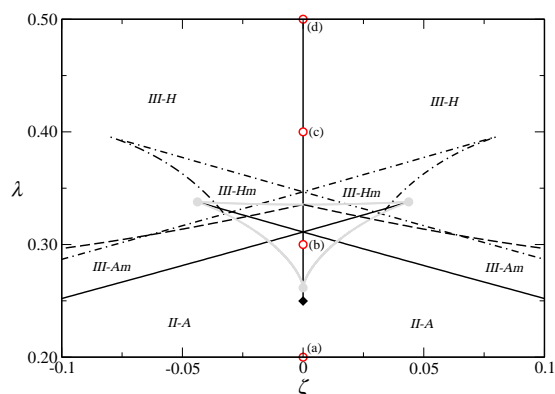
Fig. 2 Partial view of the Global Phase Diagram for Lennard-Jones mixtures composed by molecules of equal size ($\xi = 0$), as calculated from the JZG EOS.[11] (continuous black line) Tricritical line, (continuous grey line) Shield boundary region (Sh-r), (dash-dot line) Critical-Pressure Step Point (CPSP), (dashed line) III-A-H boundary. (grey circles) tricritical end points for the shield region, (black diamond) low pressure tricritical endpoint. Red points (a), (b), (c) and (d) represent the coordinates for the analysis performed in this work.

The different types of phase behavior can be unequivocally delimited by means of parametrical boundaries described by rigorous mathematical relationships (or transitional mechanisms), that have been well established either on the basis of mathematical bifurcations[42] of the Gibbs energy function or in terms of the theory of displacements.[9,43,44] Consequently, once the GPD is available - *as in the case of Lennard-Jones fluids* - force field potential parameters can be unequivocally de-

termined, for performing strategically guided molecular simulations[45–53].

Table 1 GPD coordinates, molecular parameter for pure fluids, and interaction parameters.

System	Type	ξ	ζ	λ	σ_{22}^*	ε_{22}^*	k_{12}
(a)	II	0.0	0.0	0.2	1.0	1.0	0.2
(b)	III (Sh-r)	0.0	0.0	0.3	1.0	1.0	0.3
(c)	III-H	0.0	0.0	0.4	1.0	1.0	0.4
(d)	III-H	0.0	0.0	0.5	1.0	1.0	0.5

Specifically, Table 1 reports the global coordinates, molecular parameters of the pure components ($\sigma_{22}^* = \sigma_{22}/\sigma_{11}$ and $\varepsilon_{22}^* = \varepsilon_{22}/\varepsilon_{11}$), and the interaction parameters k_{12} for a set of selected Lennard-Jones mixtures selected. In addition, Fig. 2 shows a partial view of the GPD for mixtures composed by Lennard-Jones spherical monomers of equivalent diameter that clearly indicates the global coordinates ($\lambda, \zeta, \xi = 0$) for which the example mixtures have been drawn (*e.g.* point a, b, c and d in Fig. 2).

Global coordinate can be directly related with the reduced Lennard-Jones parameters as follows:

$$
\begin{aligned}
\xi &= \frac{\sigma_{22}^3 - \sigma_{11}^3}{\sigma_{22}^3 + \sigma_{11}^3} = 0 \\
\zeta &= \frac{\varepsilon_{22}/\sigma_{22}^3 - \varepsilon_{11}/\sigma_{11}^3}{\varepsilon_{22}/\sigma_{22}^3 + \varepsilon_{11}/\sigma_{11}^3} \\
\lambda &= \frac{\varepsilon_{22}/\sigma_{22}^2 - 2\sqrt{\varepsilon_{11}\varepsilon_{22}}(1-k_{12})/\sqrt{\sigma_{11}\sigma_{22}} + \varepsilon_{11}/\sigma_{11}^2}{\varepsilon_{22}/\sigma_{22}^3 + \varepsilon_{11}/\sigma_{11}^3}
\end{aligned}
\tag{1}
$$

It has been previously reported that the EoS model used[11] exhibits pitfalls in the low and high temperature ranges due to the prediction of unphysical critical points[45,54,55]. In order to avoid the effects of these pitfalls in the predicted phase equilibrium and interfacial properties, the EoS model has been carefully treated to produce pitfall-free Types in adequate temperature ranges. Thus, the regions drawn represent the ranges shown in Fig. 2, which correspond to a combination of pure fluids molecular parameters and interaction parameters where the EoS predicts genuine Types of behavior over the interpolation range, where it was derived from molecular simulation data[11,56].

One of the most interesting phenomena found is the ability of simple models to predict four-phase equilibrium inside the shield region (Sh-r)[57,58]. As shown in Fig. 2, the Sh-r for mixtures of molecules of equal size ($\xi = 0$) is an almost triangular symmetric region where three tricritical (TC) boundaries, a critical-pressure step point (CPSP) boundary, and a limiting azeotropic-heteroazeotropic boundary (III-A-H line) converge. Boshkov and co-workers[59,60] published two papers
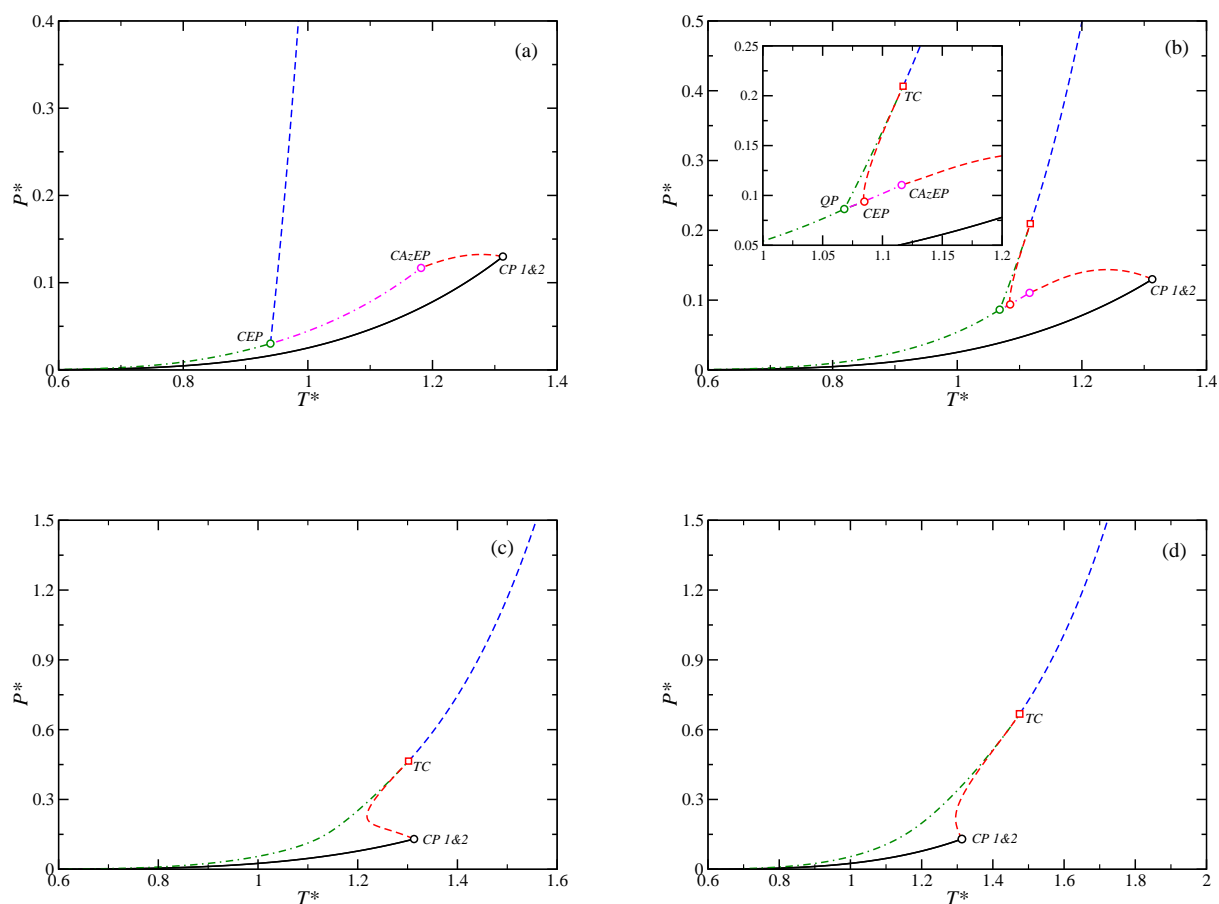
Fig. 3 Pressure ($P^* = P\sigma_{11}^3/\varepsilon_{11}$) vs temperature ($T^* = Tk_B/\varepsilon_{11}$) projection of the phase diagram for symmetrical and equal-sized Lennard-Jones mixtures, with molecular parameters taken from Table 1 and obtained from the JZG EoS [11] predictions. (a) type-II-A mixture ($\varepsilon_{12}^* = 0.8\varepsilon_{11}^*$); (b) type-III (Sh-r) mixture ($\varepsilon_{12}^* = 0.7\varepsilon_{11}^*$), (c) type-III-H mixture ($\varepsilon_{12}^* = 0.6\varepsilon_{11}^*$), (d) type-III-H mixture ($\varepsilon_{12}^* = 0.5\varepsilon_{11}^*$). (Continuous black lines) vapor pressure of the pure components (1 & 2), (dash-dot green line) LLV three-phase line, (dashed red line) vapor-liquid (VL) critical line, (dashed line) liquid-liquid (LL) critical line, (dash-dot magenta line) azeotropic line. TC, QP, CEP and CAzEP denotes the Tricritical Point, the Quadruple Point, the Critical End Point and Critical Azeotropic End Point of the mixtures, respectively. Inset: close-up of the region around QP.

concerning GPD calculations for binary Lennard-Jones fluids. Although the coordinates of the shield region were presented in the predicted GPDs, no calculation was reported for depicting the coordinates of the CPSP transition, so far. This is the first time, that a complete shield region is presented for binary Lennard-Jones fluids using the JZG-EoS[11] model. A CPSP transition[61] bounds the behavior of multiple pressure stationary points along a critical line in a $P^* - T^*$ projection. In addition, the III-A-H line masks the azeotropic behavior inside a range of immiscibility. Finally, a tricritical transition breaks the continuity of a critical line in a critical end point (CEP). Due to all these transitional mechanisms, the systems that may be found inside the Sh-r are hybrids of types II and III that may present stationary pressure points and/or azeotropic behavior. In order to describe and characterize the phase and interface topologies for different Lennard-Jones mixtures, we have selected four GPD coordinates that represent symmetrical and equal-sized Lennard-Jones mixtures in Fig. 2. Table 1 summarizes the GPD coordinates, the molecular parameters of pure components, and the interaction parameters for these mixtures and in Fig. 3 we show the critical projection in wide range of pressure and temperature. Along the $\zeta = \xi = 0$ and $\lambda \geq 0$, mixtures essentially classify as size and energy symmetric Type II-III systems, and molar isopycnic behavior[9,28] is observed between immiscible liquid phases over the whole range of immiscibility above the pressure of the three-phase line, from zero temperature up to the CEP (or, alternatively, up to the temperature of the quadruple point in the case of mixtures that belong to the shield region).

Briefly, as depicted in Fig. 3(a), the quoted type-II-A mixture is characterized by a Vapor-Liquid (VL) critical line that continuously joins the critical points of the pure constituents (CP 1 & 2) with Critical Azeotropic End Point (CAzEP). An additional critical line related to Liquid-Liquid (LL) immiscibility connects a three-phase line in an Critical End Point (CEP) from which it diverges to the high pressure range. The liquid-liquid-vapor (LLV) three-phase line is originated in the low temperature range and ending in the CEP, and finally, the Azeotropic line connects the CEP with the CAzEP. Figure 3(c) and 3(d) they are characterized by the same global behavior, where a LLV three-phase line is located at pressures above the vapor pressure curves of pure components and running from the low pressure and temperature range and ending at a Tricritical Point (TC). In addition to that, the mixture has two critical lines with different characters. The first one is a VL critical line, running from the critical point of pure components 1 and 2 to a TC. The second one is a LL critical line, running from the TC of the mixture towards high pressures and temperatures. Probably the most interesting system is calculated for the first time in Fig. 3b using the EoS model[11] for Lennard-Jones mixtures, where a particular $P^* - T^*$ projection may be found inside the Sh-r. Due to the previously mentioned

transitional mechanisms, the general trend and connectivity of the main critical lines may vary as the ζ, λ coordinates change.[62] As can be seen in the inset of Fig. 3b, the QP appears below the critical temperature of the constituents of the mixture, connecting a low-temperature three-phase line with three high-temperature three-phase lines. However, it is important to recall that, given the symmetry of the system, two three phase lines are overlapping. Also, we can observe that the pressure of the QP is larger than the vapor pressure of the pure components, and at the QP, three phases have liquid-type densities and the remaining phase has vapor-type density. This particular system exhibits three different critical lines, one VL critical line connects the critical points of the pure constituents with CAzEP, another VL critical line running from the CEP and ending at a TC of the mixture, and finally, the third one is a LL critical line, running from the TC towards high pressures and temperatures.

2.2 Simulation Details

We have also considered Molecular Dynamics (MD) simulations[63,64] in a $NP_z\mathscr{A}T$ ensemble[65], instead of the traditional NVT ensemble, owe to the ability of the former to explicitly describe the interface. In the $NP_z\mathscr{A}T$ ensemble, the number of molecules (N), the normal pressure (P_z), the interfacial area ($\mathscr{A}$) and the temperature (T) are pre-imposed simulation conditions that reflect the actual thermo-physical properties, whereas the dimensions of the simulation cell fluctuate in order to match the appropriate volume of the molecular system. Following the original work of the ensemble under consideration (for further details, the reader is referred for instance to Zhang *et al.*[65]), as well as some recent results that clearly illustrate its performance, the $NP_z\mathscr{A}T$ ensemble is one of the most effective ensembles for simulating molecular systems in liquid-liquid and liquid-supercritical fluid equilibrium conditions.[65–72] Its effectiveness may be attributed to the flexibility of the approach in calculating the appropriate dimensions of the simulation box. Molecular Dynamics simulations for binary mixtures were conducted considering more than 14000 Lennard-Jones spheres at conditions where the LL interface is present in an $NP_z\mathscr{A}T$ ensemble, using the GROMACS (version 4.6.1 in double precision) simulation open source suite[73]. The simulation cell corresponds to an $L_x \times L_y \times L_z$ parallelepiped with periodic boundary conditions in all three directions. Specifically, L_x and L_y were oriented parallel to the interfacial area, whereas L_z acted normal to the interface. The simulation cell dimensions have been selected large enough to accommodate the different liquid phases with enough molecules, thus ensuring representative bulk phases appropriately separated by a sharp interfacial region. This explicit interface simulation technique has the advantage of providing direct access to the structure of the interface, allowing

the simultaneous determination of bulk coexistence properties (densities of the present phases), different interfacial properties (*i.e.* interfacial tension, adsorption phenomena), and microscopic properties as density profiles across the interface, interface thickness, radial distribution functions, etc.

The procedure used to simulate the biphasic interfaces is the following. In the case where equilibrium between hardly immiscible phases is analyzed, the first step entails the equilibration of two independent simulation boxes. Both boxes were equilibrated in the $NP_z\mathscr{A}T$ ensemble at the pressure and temperature conditions of interest. The dimensions of the parallelepiped simulation box, L_x, L_y, and L_z, were adjusted to facilitate the subsequent assembly of a biphasic box, and thus the dimensions L_x and L_y were kept constant with a value $L_x = L_y = 14\sigma_{11}$. This way, the volume variations of the simulation box at constant temperature and pressure were performed by variations in the L_z distance, setting as an initial value $L_z = 2L_x$. The distribution of molecules N_1 and N_2 was set according to the mole fractions calculated from the JZG EoS[11]. The molecular sites N_1 and N_2 interact to each other by means of a truncated Lennard-Jones potential. The force field constant, ε_{12}, and the molecular diameter, σ_{12}, were calculated from pure parameters according to the modified version of Lorentz-Berthelot mixing rules[74,75].

$$\varepsilon_{12} = \sqrt{\varepsilon_{11}\varepsilon_{22}}(1-k_{12}) \quad ; \quad \sigma_{12} = \frac{1}{2}(\sigma_{11}+\sigma_{22}) \quad (2)$$

In order to reduce the truncation and system size effects involved in the phase equilibrium and interfacial properties calculations, the cut-off radius (r_c) has been taken equal to a large value of $7\sigma_{ii}$. It has been shown by several authors[52,76–78] that a cut-off above six segment diameters provides a reliable description for the pressure and interfacial properties of the Lennard-Jones fluid. Once both boxes were equilibrated, a slab composed of the N_1 simulation box in the middle and two replicas of the N_2 box at both ends in the z direction was assembled, by simply displacing the appropriate value of the z coordinate for both N_2 boxes. This yielded an inhomogeneous simulation box containing two explicit interfaces between both fluids. Once the biphasic box was constructed, it was allowed to evolve under NVT conditions until the interface was equilibrated, which usually took an average of 5 ns. After that the simulations so-prepared were then run in the $NP_z\mathscr{A}T$ ensemble during 20 ns (including an equilibration period of 10 ns), where a specifying Verlet leapfrog[79] algorithm with a time step of 0.002 ps has been used. Following recommendations of Herdes *et al.*[46], the Berendsen thermostat and barostat[80] were selected as the coupling algorithms for the $NP_z\mathscr{A}T$ simulations.

Interfacial properties, such as concentration along the interfacial region $(\rho_i(z))$ and interfacial tension (γ), can be directly calculated from MD simulations. Concentration profiles, $\rho_i(z)$, were calculated by dividing the system in 250 slabs along the z direction, assigning the position of each Lennard-Jones center, z_i, to the corresponding slab and constructing then the molecular concentration from a mass conservation constraint. The interfacial tension, γ, is obtained using the mechanical route[34,81–83] given by:

$$\gamma = \frac{L_z}{2}\left[P_{zz} - \frac{P_{xx}+P_{yy}}{2}\right] \quad (3)$$

where $P_{\alpha\alpha}$ is an element of the pressure tensor in the x-, y-, z-direction. Particularly, P_{zz} is the normal component of the pressure tensor (or the equilibrium pressure, $P_{zz} = P_z$), the additional factor $1/2$ comes from having two interfaces in the system, and L_z is the size of the simulation box in the z direction, defined along the longitudinal dimension across the interface. In order to estimate errors on the variables computed, the sub-blocks average method has been applied[80]. In that approach, the production period is divided into n independent blocks. The statistical error is then deduced from the standard deviation of the average $\bar{\sigma}/\sqrt{M}$, where $\bar{\sigma}$ is the variance of the block averages and M has been fixed, in this work to M=10. All the quantities in our paper are expressed in conventional reduced units of component 1, with σ_{11} and ε_{11} being the length and energy scaling units, respectively. Thus, $T^* = Tk_B/\varepsilon_{11}$, $P^* = P\sigma_{11}^3/\varepsilon_{11}$, $\rho^* = \rho\sigma_{11}^3$, $\gamma^* = \gamma\sigma_{11}^2/\varepsilon_{11}$ and $z^* = z/\sigma_{11}$.

3 Results

In this section, we present, analyze, and discuss the main results from the simulations for the liquid-liquid interface of the symmetrical mixture of equal-sized LJ spherical molecules, which exhibit phase density inversion. We focus on the interfacial properties such as density profiles, and surface tension. In particular, we examine the pressure, P^* and mixture dispersive energy, ε_{12}^* dependence of these properties. In addition, we also analyze the interfacial structure of asymmetrical Lennard-Jones mixtures, with the same density inversion phenomena.

Let us focus now our attention to the characteristics of the interfacial behavior, namely density profiles and interfacial tensions, which were calculated from MD using the $NP_z\mathscr{A}T$ ensemble. In this case, the depicted results for density profiles have been taken from half of the simulation box, in order to avoid unnecessary repetitions. Also for convenience, all density profiles have been shifted along z axis to place z_0 at the origin. The equilibrium density profiles of each of the mixture components, as well as the total density, are computed from averages of the histogram of densities along the z^* direction over the production stage. The two bulk liquid densities of both components and the total density are obtained
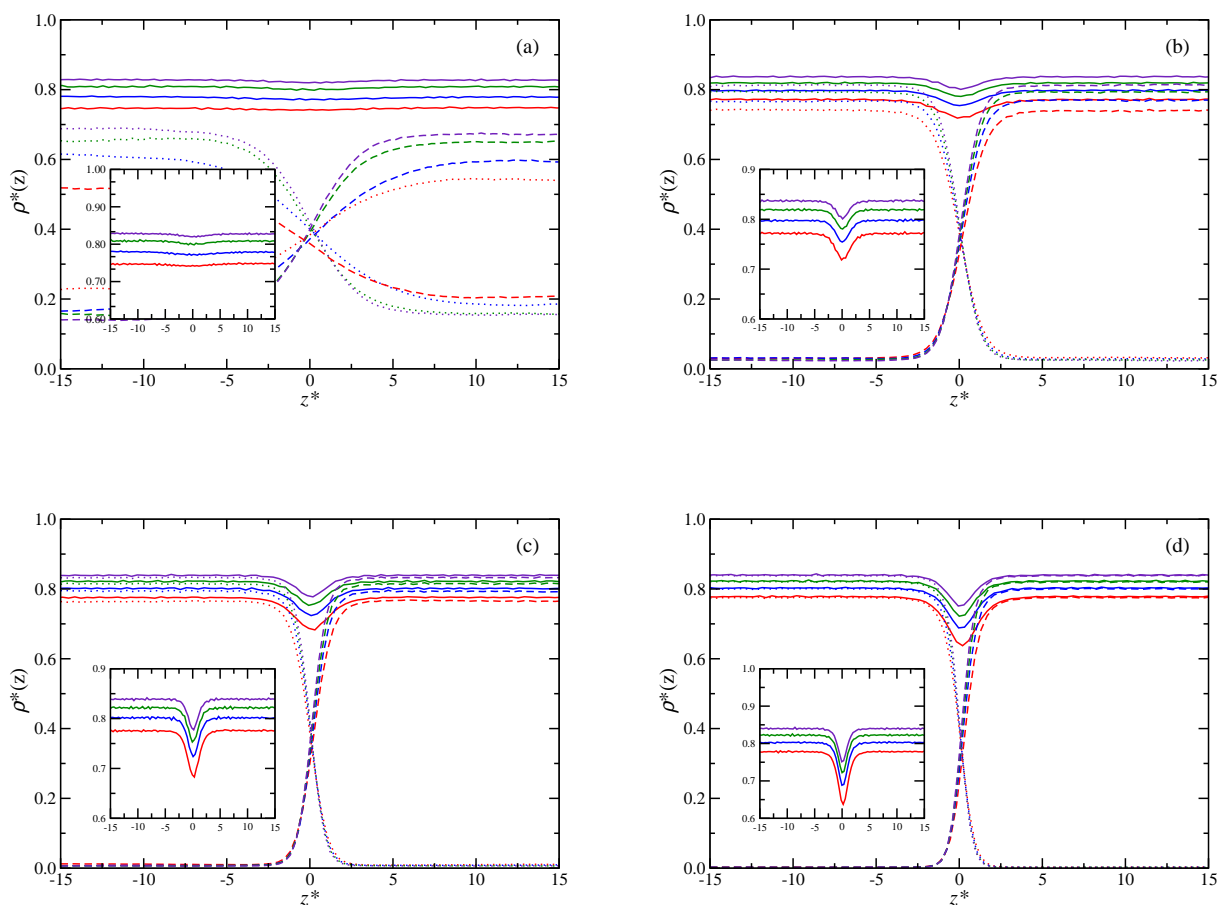
Fig. 4 Simulated equilibrium density profiles for the mixture (continuous curves), component 1 (dotted curves), and component 2 (dashed curves), across the liquid-liquid interface of the symmetrical mixture of equal-sized LJ spherical molecules, at $T^* = 0.9$ and different equilibrium pressures. (a) type-II-A mixture ($\varepsilon_{12}^* = 0.8\varepsilon_{11}^*$); (b) type-III Sh-r mixture ($\varepsilon_{12}^* = 0.7\varepsilon_{11}^*$), (c) type-III-H mixture ($\varepsilon_{12}^* = 0.6\varepsilon_{11}^*$), (d) type-III-H mixture ($\varepsilon_{12}^* = 0.5\varepsilon_{11}^*$). Pressure of the system increases from bottom up in the total density profile ($P^* = 0.3, 0.6, 0.9, 1.2$). Note that curves with the same color correspond to the same pressure value. Inset: Details of simulated total density profiles.

Table 2 Density of component 1 at liquid L_1, $\rho_1^{*L_1}$, density of component 2 at liquid L_1, $\rho_2^{*L_1}$, molar composition of component 1 at liquid L_1, $x_1^{L_1}$, density of component 1 at liquid L_2, $\rho_1^{*L_2}$, density of component 2 at liquid L_2, $\rho_2^{*L_2}$, molar composition of component 1 at liquid L_2, $x_1^{L_2}$ and interfacial tension, γ^*, calculated from mechanical route given by eqn (3) at $T^* = 0.9$, different pressures of the system, P^*, and different dispersive energy between unlike species, $\varepsilon_{ij}^* = (1 - k_{ij})\varepsilon_{ii}^*$ for the symmetrical mixture of equal-sized LJ spherical molecules. As defined in Section 2.2 all quantities are expressed in reduced units and the errors are estimated as explained in the text.

P^*	$\rho_1^{*L_1}$	$\rho_2^{*L_1}$	$x_1^{L_1}$	$\rho_1^{*L_2}$	$\rho_2^{*L_2}$	$x_1^{L_2}$	γ^*
				$\varepsilon_{12}^* = 0.8\varepsilon_{11}^*$			
0.3	0.5291(9)	0.2282(2)	0.699(1)	0.2193(9)	0.5193(2)	0.297(6)	0.027(7)
0.6	0.6144(4)	0.1851(2)	0.769(4)	0.1664(4)	0.5941(2)	0.218(4)	0.039(9)
0.9	0.6581(4)	0.1612(2)	0.805(3)	0.1516(3)	0.6483(3)	0.188(1)	0.063(7)
1.2	0.6822(6)	0.1557(2)	0.814(8)	0.1461(5)	0.6721(2)	0.1789(11)	0.075(8)
				$\varepsilon_{12}^* = 0.7\varepsilon_{11}^*$			
0.3	0.7416(1)	0.0315(7)	0.959(8)	0.0303(6)	0.7401(2)	0.039(9)	0.397(1)
0.6	0.7666(12)	0.0290(8)	0.964(1)	0.7687(1)	0.0308(8)	0.038(1)	0.450(11)
0.9	0.7938(15)	0.0259(5)	0.968(2)	0.0253(5)	0.7930(11)	0.031(7)	0.519(1)
1.2	0.8122(2)	0.0237(6)	0.972(7)	0.0247(9)	0.8132(14)	0.029(5)	0.550(9)
				$\varepsilon_{12}^* = 0.6\varepsilon_{11}^*$			
0.3	0.7653(23)	0.0103(6)	0.980(4)	0.0163(21)	0.7662(1)	0.020(8)	0.752(2)
0.6	0.7943(12)	0.008(6)	0.989(2)	0.007(3)	0.7926(1)	0.009(1)	0.842(4)
0.9	0.8149(13)	0.0064(3)	0.992(2)	0.0068(2)	0.8155(13)	0.008(3)	0.912(1)
1.2	0.8326(1)	0.0066(2)	0.992(1)	0.0064(3)	0.8324(11)	0.007(6)	0.965(3)
				$\varepsilon_{12}^* = 0.5\varepsilon_{11}^*$			
0.3	0.7751(1)	0.0031(2)	0.996(1)	0.0032(2)	0.7753(11)	0.004(1)	1.061(15)
0.6	0.8004(9)	0.0025(2)	0.996(9)	0.0024(1)	0.8001(11)	0.003(3)	1.152(2)
0.9	0.8207(14)	0.002(3)	0.997(4)	0.0018(1)	0.8205(10)	0.002(2)	1.251(1)
1.2	0.8381(12)	0.002(2)	0.997(9)	0.0018(1)	0.8381(1)	0.002(1)	1.319(3)

by averaging $\rho_1^*(z)$, $\rho_{2*}(z)$, and $\rho^*(z)$, respectively over appropriate regions sufficiently removed from the interfacial region. The densities obtained are meaningful since the central region of each liquid slab is thick enough at all pressures. The other phase of bulk liquid densities is obtained after averaging the corresponding density profiles on both sides of the central slab. The statistical uncertainty of these values is estimated from the standard deviation of the mean values. In order to analyze the interfacial properties of mixtures with different dispersive energy between unlike species ($\varepsilon_{ij}^* = (1 - k_{ij})\varepsilon_{ii}^*$), we have selected the same temperature for each system, focusing in the large liquid-liquid region observed on the VLLE in Fig. 3 for each system. A detailed description of the evolution of these symmetric systems is explained in the work of Martinez-Ruiz *et.al.* [28]

The quoted Fig. 4 shows the evolution of the interfacial density profiles $\rho_1^*(z)$, $\rho_2^*(z)$, and $\rho^*(z)$ at $T^* = 0.9$ in the range of pressure conditions indicated in Table 2. It is important to remark that, due to the symmetry of the mixtures, bulk liquid total densities associated to both liquid phases are identical. In fact, partial density profiles of both components, summarized in Table 2, should be balanced in each of the phases, as can be seen in Fig. 4, or in other words they are symmetrical with each other. The interfacial behavior of the total density profile for each mixture deserves special attention. It happens to be nearly constant in the bulk region of the liquid phases, but exhibits a local minimum at the interface, when passing from one liquid phase to the other. This condition is obvious in this kind of mixtures, because as explained previously in Fig. 1, for a hypothetical binary mixture that exhibits density inversion, the coordination of the equal bulk densities phases implies a drastic distortion of the mixture density profiles. For the particular case of these mixtures, we can also point out that there is no interfacial adsorption of the lighter component of the mixture, as the pure compound profiles show the classical *tanh* shape. However, the total density profile along the interface shows the development of a structure type of interfacial adsorption (See Fig. 1(b)), due to the promotion of total desorption point condition ($d\rho_1/d\rho_2 = -1$; $d\rho/dz = 0$ and $d^2\rho_1/d\rho_2^2 > 0$ in the interfacial region). A similar behavior has been previously observed for liquid-liquid interfaces in partially miscible mixtures of LJ-like systems from MD simulation [28,84–86], Density Functional Theory [86,87] and Square Gradient Theory [88].

Focusing on the interfacial region in Fig. 4, we can see that the total desorption increases when the interaction parameter in mixture also increases, or the dispersive energy between unlike species decreases (remember that $\varepsilon_{12} = (1 - k_{12})\varepsilon_{11}$). From a thermodynamic point of view, when the dispersive energy parameter of the mixture decreases, the system becomes more immiscible, which is clearly reflected in the partial den-
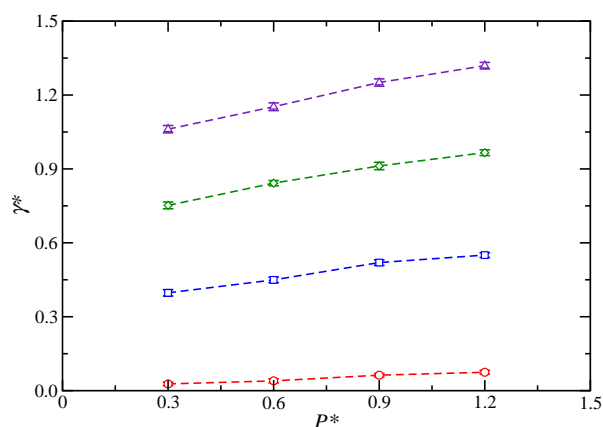
Fig. 5 Liquid-liquid interfacial tension as a function of pressure for symmetrical mixture of equal-sized LJ spherical molecules with different dispersive energy between unlike species, $\varepsilon_{ij}^* = (1 - k_{ij})\varepsilon_{ii}^*$ at $T = 0.9$. Different symbols and colors represent the interfacial tension obtained from $NP_z \mathscr{A} T$ MD simulations using the mechanical route given by eqn (3). (open circles) $\varepsilon_{12}^* = 0.8\varepsilon_{11}^*$; (open squares) $\varepsilon_{12}^* = 0.7\varepsilon_{11}^*$, (open diamonds) $\varepsilon_{12}^* = 0.6\varepsilon_{11}^*$, (open triangles) $\varepsilon_{12}^* = 0.5\varepsilon_{11}^*$. The curves are included as guide.

sities profiles. The inset in Fig. 4 highlights the layer of desorbed molecules in the total density profiles. The enhanced desorption is clear from these figures. It is expected also that desorption decreases with increasing pressure, however Fig. 4(a) displays a different effect in the interfacial behavior. In fact, when pressure increases desorption increases generating a completely flat profile at very low pressures. We think that this phenomenon is directly related to the global phase transition when the selection of dispersive interactions between unlike species of the symmetrical binary mixture crosses the shield region. It is important to point out that this reasoning is based on the results obtained by Mejía and Segura[62] by combining Square Gradient Theory with the van der Waals equation of state. The quoted authors show that an evolution in the shield region, taken $\zeta = 0$ and varying λ produces a shape transition point on density profiles and yields a singularity for the $\partial \rho_1 / \partial \rho_2$ derivative. As an additional comparison, Figs. 4(b)-(d) show that the desorption in the total density profile decreases as pressure increases, as shown also by the results of Martinez-Ruiz *et.al.*[28] in other thermodynamics conditions for liquid-liquid systems.

The pressure dependence of the interfacial tension for mixtures of LJ molecules interacting with different dispersive energy parameters between unlike species, ε_{12}, is shown in Fig. 5. At any given pressure, the interfacial tension is larger

Table 3 Molecular properties and interaction parameter for the asymmetrical Lennard-Jones mixture depicted in Fig. 6

Type	$\sigma_{22}^3/\sigma_{11}^3$	$\varepsilon_{22}/\varepsilon_{11}$	k_{12}
III	2.000	2.000	0.1818

for smaller dispersive energy parameter. Once again, this is consistent with the larger interaction parameters in systems consisting of symmetrical mixture of equal-sized LJ spherical molecules. As can be seen from Fig. 5, an essentially linear behavior is found for the range of pressures considered. We can conclude that this effect on the interfacial tension is consistent with the larger dispersive energy parameter in systems with liquid-liquid equilibrium.
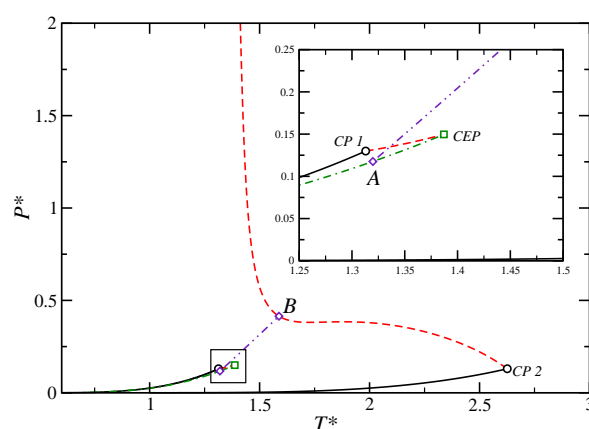

Fig. 6 $P^* - T^*$ critical projection for a Lennard-Jones binary mixture with properties indicated in Table 3. (Continuous black lines) vapor pressure of the pure components (1 & 2), (dash-dot green line) LLV three-phase line, (dashed red line) vapor-liquid (VL) critical line, (dashed line) liquid-liquid (LL) critical line, (dash-dot-dot indigo line) density inversion line. Inset: close-up of the region around the Critical End Point (CEP).

In the results previously shown, we demonstrated the predictive ability of molecular simulation on the characterization of phase and interface behavior in mixtures that exhibit the phenomenon of phase inversion. In particular the effect of dispersive energy parameters to generate different local minimum values at the interface has been demonstrated. However, structures with adsorption on the interface probably can not exist for symmetric and equal-size systems. In order to find some evidence of adsorption in the total profiles, we have decided to focus again on the interfacial properties that, on the basis of statistical mechanics considerations given by the EoS model and MD simulations, turn out to be the most affected

by conformational parameters.

Let us consider then the binary mixture with the molecular properties and interaction parameters indicated in Table 3[9], whose equilibrium conditions have been illustrated in the $P^* - T^*$ projection shown in Fig. 6. This selected mixture exhibits Type III-m behavior from the classification of van Konynenburg and Scott.[31], case in which one of the VL critical branches emerges from the most volatile component (component 1 in this case) and then evolves to a critical end point (CEP), where it connects the critical point of a three-phase line. A second critical line begins at the critical point of the heavier component (component 2), and then diverges to the high pressure range. Besides the details concerning the connectivity of critical lines, Type-III mixtures present a three-phase line characterized by a VLLE running from the low pressure and temperature range and ending at a critical end point (CEP). A density inversion line between two liquid phases appears along the three phase line, thus constraining the stability of the liquid-liquid equilibrium (Point A) to a critical end point (point B). This confirms unequivocally a range of molar isopycnicity for the case under consideration, while in symmetric systems the isopycnic behavior is observed between immiscible liquid phases over the whole immiscibility range above the pressure of the three-phase line, from low temperature up to the CEP. In this particular system it is interesting to explore how the characteristics of density inversion may affect the interfacial structure, because molar isopycnicity annihilates the differences between bulk phase densities (as it happens at the immediacy of any critical point). As observed in Fig. 7, the density envelopes in a $(T^* - \rho^*)$ projection at $P^* = 0.25$ reveal that both phases present the same molar density in non-critical conditions.

Table 4 Total density at liquid L_1, ρ^{*L_1}, total density at liquid L_2, ρ^{*L_2}, and interfacial tension, γ^*, calculated from mechanical route given by eqn (3) at $P^* = 0.25$ and different temperatures T^*. As defined in Section 2.2 all quantities are expressed in the reduced units and the errors are estimated as explained in the text.

$T*$	ρ^{*L_1}	ρ^{*L_2}	γ^*
1.4	0.488(3)	0.506(8)	0.0174(11)
1.44	0.482(6)	0.482(1)	0.0228(15)
1.5	0.478(9)	0.416(7)	0.0347(21)

Certainly, along the phase envelope the total density profiles should show a temperature driven abrupt change in their configuration, to generate a state of equal density. According to Fig. 7, we have selected three thermodynamic conditions allowing to characterize a phase density inversion. As in symmetrical mixtures, $NP_z\mathscr{A}T$ MD simulation has been used. Fig. 8 collects the MD results for the $z^* - \rho^*$ profiles at the three equilibrium conditions described previously in Fig. 7. This Figure shows the evolution of the interfacial density profiles

of the components and the mixture for the temperatures listed in Table 4. Results from the phase densities and interfacial tensions are presented in Table 4.
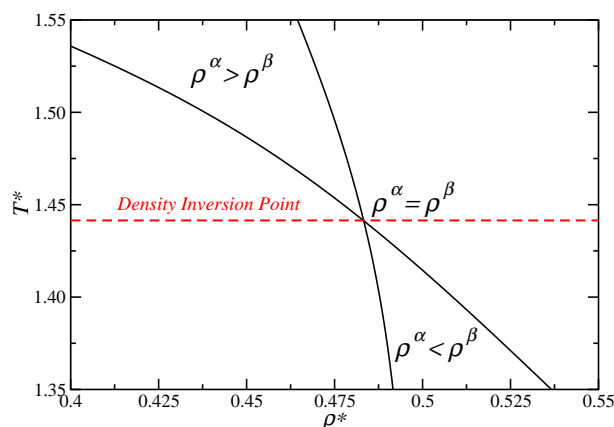

Fig. 7 $T^* - \rho^*$ projection for a Lennard-Jones binary mixture with properties indicated in Table 3 at $P^* = 0.25$. (continuous lines) JZG EoS[11] prediction

A detailed inspection of density profiles diagram reveals clear evidence of density inversion upon increasing temperature at constant pressure, a condition that is confirmed by MD calculations. By comparing the interfacial structures in pre (Fig. 8(a)) and post (Fig. 8(c)) density inversion condition, we deduce that density inversion point implies a drastic distortion of the mixture density profiles, as we had assumed in cases shown in Fig. 1. It is interesting to note that the profiles of both components are represented roughly by the traditional shape of the hyperbolic tangent function, case in which no selective adsorption is observed, but nevertheless the total density profile exhibits a -subtle but clear,- maximum at the interface, highlighted in the inset of Fig. 8(b). To our knowledge, this is the first time that mixtures with accumulation at the interface (total density profiles) are calculated by molecular simulation. Finally, as complementary MD simulations results, we can see from Table 4, that interfacial tension increases as temperature increases.

4 Concluding Remarks

This work has been devoted to develop an accurate characterization for describing the liquid-liquid interfacial behavior in binary Lennard-Jones mixtures. Particular emphasis has been placed on describing characteristics of the density profiles in thermodynamics condition were phase density inversion is present, in direct relation with the properties of its
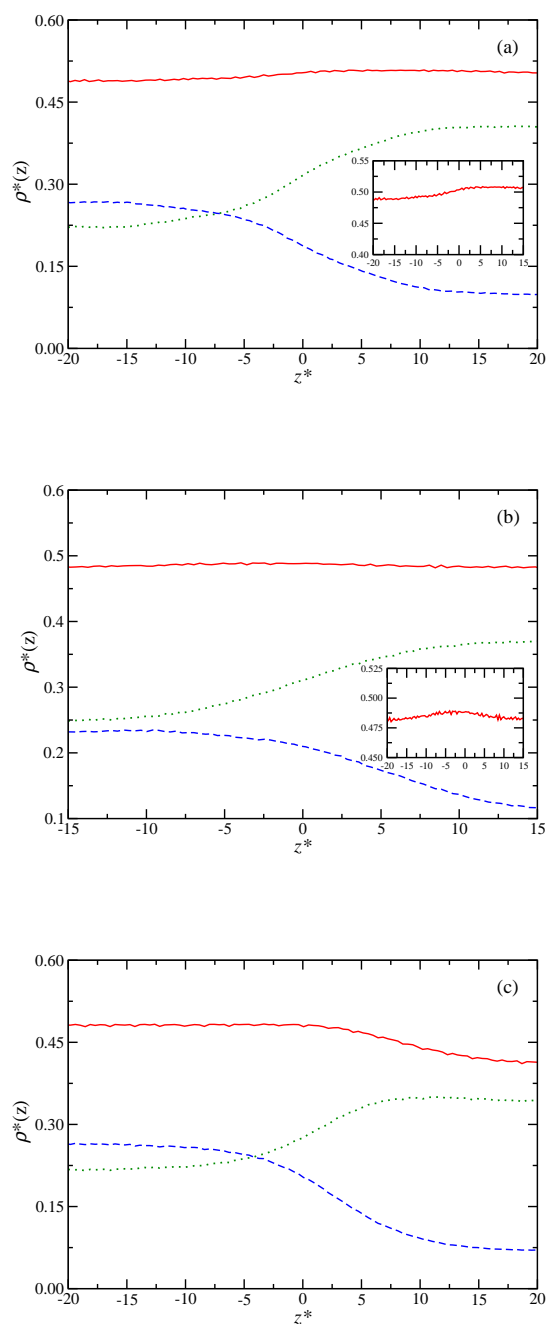
Fig. 8 Simulated equilibrium density profiles of the mixture (continuous red curves), component 1 (dotted green curves), and component 2 (dashed blue curves), across the liquid-liquid interface for a Lennard-Jones binary mixture with properties indicated in Table 3 at $P^* = 0.25$. (a) $T^* = 1.40$, (b) $T^* = 1.44$ (c) $T^* = 1.5$. Inset: Detail of simulated total density profiles

constituent binaries (*i.e.* σ_{ii}, ε_{ii} and k_{ij}). The molecular parameters of the quoted binaries were chosen from the GPD of Lennard-Jones fluids composed by molecules of equal size which, in turn, were predicted by using the JZG EoS. The complex behavior of phase density inversion is carried out by exploiting the direct link with the underlying intermolecular potential and the corresponding EoS model, using direct MD simulation in the $NP_z\mathscr{A}T$ ensemble. From our results, we have demonstrated its clear influence of phase density inversion phenomena on the interfacial structure. From an interfacial structure viewpoint, isopycnic mixtures -characterized by the same molar density- introduce a drastic distortion on the total density profile, an effect that may be controlled by directly changing the thermo-mechanical conditions of the phase equilibrium about the isopycnic condition. Particularly, it has been found that density inversion produce a desorption phenomena along the interfacial zone in binary systems composed by equal-size molecules. Moreover, adsorption phenomena appears when the asymmetry of the system increases. Finally, it is interesting to note that the present mechanisms -desorption/adsorption along the interfacial zone- may induced only for the existence and persistence of density inversion behavior.

5 Acknowledgements

References

1 J. L. Sengers, *Fluid Phase Equilib.*, 1999, **158–160**, 3–17.

2 G. M. Schneider, A. L. Scheidgen and S. Klante, *Ind. Eng. Chem. Res.*, 2000, **39**, 4476–4480.

3 J. L. Sengers, *J. Supercrit. Fluids*, 2006, **39**, 144–153.

4 S. E. Quiñones-Cisneros, *Phys. Chem. Chem. Phys*, 2004, **6**, 2307–2313.

5 J. L. Sengers, *Condens. Matter*, 2009, **21**, 164222–164232.

6 H. Quinteros-Lama, G. Pisoni, J. M. Garrido, A. Mejía and H. Segura, *Fluid Phase Equilib.*, 2015, **394**, 175–185.

7 S. E. Quiñones-Cisneros, *MSc thesis*, University of Minnesota, 1987.

8 S. E. Quiñones-Cisneros, *Fluid Phase Equilib.*, 1997, **135**, 103–112.

9 J. M. Tardón, J. M. Garrido, H. Quinteros-Lama, A. Mejía and H. Segura, *Fluid Phase Equilib.*, 2012, **336**, 84–97.

Physical Chemistry Chemical Physics Accepted Manuscript

10 J. S. Rowlinson and F. L. Swinton, *Liquids and Liquids Mixtures*, Butterworth, London, 1982.

11 J. Johnson, J. A. Zollweg and K. E. Gubbins, *Mol. Phys.*, 1993, **78**, 591–618.

12 A. Galindo, L. A. Davies, A. Gil-Villegas and G. Jackson, *Mol. Phys.*, 1998, **93**, 241–252.

13 A. Gil-Villegas, A. Galindo, P. J. Whitehead, S. J. Mills, G. Jackson and A. N. Burgess, *J. Chem. Phys.*, 1997, **106**, 4168–0000.

14 J. Gross and G. Sadowski, *Ind. Eng. Chem. Res.*, 2001, **40**, 1244–1260.

15 T. Lafitte, A. Apostolakou, C. Avendaño, A. Galindo, C. S. Adjiman, E. A. Müller and G. Jackson, *J. Chem. Phys.*, 2013, **139**, 154504–154540.

16 S. E. Quiñones-Cisneros, J. García, J. Fernández and M. A. Monsalvo, *Int. J. Refrigeration*, 2005, **28**, 714–724.

17 S. Aparicio-Martinez and K. R. Hall, *Ind. Eng. Chem. Res.*, 2007, **46**, 273–284.

18 S. Aparicio-Martinez and K. R. Hall, *Ind. Eng. Chem. Res.*, 2007, **46**, 291–296.

19 J. García, X. Paredes and J. Fernández, *J. Supercrit. Fluids*, 2008, **45**, 261–271.

20 M. Flores, M. J. Tardón, C. Bidart, A. Mejía and H. Segura, *Fluid Phase Equilib.*, 2012, **313**, 171–181.

21 E. Brunner, *J. Chem. Thermodyn*, 1990, **22**, 335–353.

22 E. Brunner, M. C. Thies and G. M. Schneider, *J. Supercrit. Fluids*, 2006, **39**, 160–173.

23 C. Bidart, H. Segura and J. Wisniak, *Ind. Eng. Chem. Res.*, 2007, **46**, 947–954.

24 S. Aparicio-Martinez, *J. Supercrit. Fluids*, 2008, **46**, 10–20.

25 J. L. Chen, *PhD thesis*, Rice University, 1989.

26 J. B. A. Paulo and D. E. Hadjiev, *Ind. Eng. Chem. Res.*, 2006, **11**, 3821–3829.

27 D. Valegol, S. Shori and C. E. Snyder, *Ind. Eng. Chem. Res.*, 2009, **48**, 2414–2421.

28 F. J. Martínez-Ruiz, A. I. M.-V. Bravo and F. J. Blas, *J. Chem. Phys.*, 2015, **143**, 104706–104717.

29 A. Mejía, *PhD thesis*, Universidad de Concepción, 2004.

30 C. Cumicheo, M. Cartes, H. Segura, E. A. Müller and A. Mejía, *Fluid Phase Equilib.*, 2014, **380**, 82–92.

31 P. H. van Konynenburg and R. L. Scott, *Philos. Trans. R. Soc. London, Ser. A*, 1980, **298**, 495–540.

32 R. Defay and I. Prigogine, *Surface Tension and Adsorption*, Longmans, London, 1966.

33 D. Henderson, *Fundamentals of Inhomogeneous Fluids*, Dekker, New York, 1992.

34 J. S. Rowlinson and B. Widom, *Molecular Theory of Capillarity*, Clarendon, Oxford, 1982.

35 R. L. Rowley, *Statistical Mechanics for Thermophysical Property Calculations*, Prentice Hall, New Jersey, 1994.

36 Q. Chen and D. Li, *Wear*, 2003, **255**, 78–84.

37 M. Najafi and A. Maghari, *J. Solution Chem.*, 2009, **38**, 685–694.

38 A. Kongkanand, *J. Phys. Chem. C*, 2011, **115**, 11318–11325.

39 D. S. Walker and G. L. Richmond, *J. Phys. Chem. C*, 2008, **112**, 201–209.

40 P. Grosfils and J. F. Lutsk, *J. Chem. Phys.*, 2009, **130**, 054703–054708.

41 A. Bolz and U. K. D. abd C. J. Peters ans T. W. De Loos, *Pure Appl. Chem.*, 1998, **70**, 2233–2258.

42 L. Z. Boshkov, *Ber. Bunsenges. Phys. Chem.*, 1992, **96**, 940–943.

43 W. Malesinski, *Azeotropy and Other Theoretical Problems of Vapour-Liquid Equilibrium*, New York Interscience, 1965.

44 J. M. Garrido, H. Quinteros-Lama, A. Mejía, J. Wisniak and H. Segura, *Energy*, 2012, **45**, 888–899.

45 J. M. Garrido, H. Quinteros-Lama, M. M. Piñeiro, A. Mejía and H. Segura, *J. Chem. Phys.*, 2014, **141**, 014503–014515.

46 C. Herdes, T. S. Totton and E. A. Müller, *Fluid Phase Equilib.*, 2015, **406**, 91–100.

47 A. Mejía, C. Herdes and E. A. Müller, *Ind. Eng. Chem. Res.*, 2014, **53**, 4131–4141.

48 A. Mejía, M. Cartes, H. Segura and E. A. Müller, *J. Chem. Eng. Data*, 2014, **50**, 2928–2941.

49 J. M. Míguez, J. M. Garrido, F. J. Blas, H. Segura, A. Mejía and M. M. Piñeiro, *J. Phys. Chem. C*, 2014, **118**, 24504–24519.

50 E. A. Müller and A. Mejía, *J. Phys. Chem. Lett*, 2014, **5**, 1267–1271.

51 E. A. Müller and G. Jackson, *Ann. Rev. Chem. Biomol. Eng*, 2014, **5**, 405–427.

52 A. Mejía, J. C. Pàmies, D. Duque, H. Segura and L. F. Vega, *J. Chem. Phys.*, 2005, **123**, 034505–034514.

53 A. Mejía and L. F. Vega, *J. Chem. Phys.*, 2006, **124**, 244505–244512.

54 I. Polishuk, *Fluid Phase Equilib.*, 2010, **298**, 67–74.

55 H. Segura, T. Kraska, A. Mejía, J. Wisniak and I. Polishuk, *Ind. Eng. Chem. Res.*, 2003, **42**, 5662–5673.

56 J. K. Johnson, E. A. Müller and K. E. Gubbins, *J. Phys. Chem*, 1994, **98**, 6413–6419.

57 D. Furman and R. B. Griffiths, *Phys. Rev. A*, 1978, **17**, 1139–1148.

58 I. C. Wei and R. L. Scott, *J. Statist. Phys*, 1988, **52**, 1315–1324.

59 L. A. Boshkov and V. A. Mazur, *Phys. Lett.*, 1984, **104**, 415–418.

60 V. A. Mazur, L. Z. Boshkov and V. G. Murakhovsy, *Russ. J. Phys. Chem.*, 1986, **60**, 29–33.

61 M. Flores, H. Segura, M. J. Tardón, J. Wisniak and I. Polishuk, *J. Supercrit. Fluids*, 2009, **48**, 108–119.

62 A. Mejía and H. Segura, *Int. J. Thermophys.*, 2005, **26**, 13–29.

63 D. Frenkel and B. Smit, *Understanding Molecular Simulation*, Academic Press, New York, 2002.

64 M. P. Allen and D. J. Tildesley, *Computer Simulation of Liquids*, Oxford University Press, New York, 1987.

65 Y. Zhang, S. E. Feller, B. R. Brooks and R. W. Pastor, *J. Chem. Phys.*, 1995, **103**, 10252–10266.

66 J. C. Neyt, A. Wender, V. Lachet and P. Malfreyt, *J. Phys. Chem. C*, 2012, **116**, 10563–10572.

67 J. C. Neyt, A. Wender, V. Lachet, A. Ghoufi and P. Malfreyt, *J. Chem. Phys.*, 2013, **139**, 024701–024711.

68 J. C. Neyt, A. Wender, V. Lachet, A. Ghoufi and P. Malfreyt, *J. Chem. Theory Comput.*, 2014, **10**, 1887–1899.

69 A. Ghoufi, F. Goujon, V. Lachet and P. Malfreyt, *J. Chem. Phys.*, 2008, **128**, 154716–154731.

70 F. Biscay, A. Ghoufi and P. Malfreyt, *J. Chem. Phys.*, 2011, **134**, 044709–044718.

71 F. Biscay, A. Ghoufi, V. Lachet and P. Malfreyt, *J. Chem. Phys.*, 2009, **131**, 124707–124722.

72 J. M. Garrido, L. Cifuentes, M. Cartes, H. Segura and A. Mejía, *J. Supercrit. Fluids*, 2014, **89**, 78–88.

73 D. V. D. Spoel, E. Lindahl, B. Hess, G. Groenhof, A. E. Mark and H. J. Berendsen, *J. Comput. Chem.*, 2005, **26**, 1701–1718.

74 H. A. Lorentz, *Ann. Phys. (Berlin)*, 1881, **12**, 127–136.

75 D. Berthelot, *R. Hebd, Seanc. Acad. Sci.*, 1898, **126**, 1703–1855.

76 D. Duque, J. C. Pàmies and L. F. Vega, *J. Chem. Phys.*, 2004, **121**, 11395–11401.

77 G. Galliero, M. M. Piñeiro, B. Mendiboure, C. Miqueu, T. Lafitte and D. Bessières, *J. Chem. Phys.*, 2009, **130**, 104704–104713.

78 J. M. Míguez, M. M. Piñeiro and F. J. Blas, *J. Chem. Phys.*, 2013, **138**, 034707–034716.

79 M. A. Cuendet and W. F. van Gunsteren, *J. Chem. Phys.*, 2007, **127**, 184102–184109.

80 H. J. C. Berendsen, J. P. M. Postma, W. F. van Gunsteren, A. di Nola and J. R. Haak, *J. Chem. Phys.*, 1984, **81**, 3684–3690.

81 H. Hulshof, *Ann. Phys. (Berlin)*, 1901, **4**, 165–186.

82 E. de Miguel and G. Jackson, *J. Chem. Phys.*, 2006, **125**, 164109–164120.

83 E. de Miguel and G. Jackson, *Mol. Phys.*, 2006, **104**, 3717–3734.

84 S. Toxvaerd and J. Stecki, *J. Chem. Phys.*, 1995, **102**, 7163–7168.

85 E. Díaz-Herrera, J. Alejandre, G. Ramírez-Santiago and F. Forstmann, *J. Chem. Phys.*, 1999, **110**, 8084–8089.

86 P. Geysermans, N. Elyeznasni and V. Russier, *J. Chem. Phys.*, 2005, **123**, 204711–204719.

87 I. Napari, A. Laaksonena, V. Talanquer and D. W. Oxtoby, *J. Chem. Phys.*, 1999, **110**, 5906–5912.

88 M. J. Tardón, *PhD thesis*, 2012, Universidad de Concepción.